

Article

Determination of the Metastable Zone Width and Nucleation Parameters of Succinic Acid for Electrochemically Induced Crystallization

Christian Kocks ^{*} , Christina Maria Krekel, Marcel Gausmann  and Andreas Jupke 

AVT—Fluid Process Engineering, RWTH Aachen University, Forckenbeckstraße 51, 52074 Aachen, Germany; christina.krekel@rwth-aachen.de (C.M.K.); marcel.gausmann@avt.rwth-aachen.de (M.G.); andreas.jupke@avt.rwth-aachen.de (A.J.)

* Correspondence: christian.kocks@avt.rwth-aachen.de

Abstract: Electrified downstream processes for biotechnologically produced carboxylic acids reduce waste salt generation significantly and make biotechnological production ecologically and economically more attractive. In order to design, optimize, scale-up and control electrochemically induced crystallization processes, knowledge of the metastable zone width (MSZW) is essential. An optical observation approach of nucleation processes close to the electrode and determination of the MSZW is presented. This work presents a method for MSZW measurements for electrochemically induced pH-shift crystallization processes by monitoring the nucleation, the saturation pH value and saturation concentration for different current densities. The measured MSZWs for electrochemically induced pH-shift crystallization are narrow due to the foreign surface, gas bubbles and electrode surface, and rising current densities lead to even smaller MSZW. Nucleation parameters are estimated from MSZW data, adapting the classical approach of Nývlt to electrochemically induced crystallization.

Keywords: electrochemically induced crystallization; succinic acid; electrified downstream processes; nucleation; pH-shift



Citation: Kocks, C.; Krekel, C.M.; Gausmann, M.; Jupke, A. Determination of the Metastable Zone Width and Nucleation Parameters of Succinic Acid for Electrochemically Induced Crystallization. *Crystals* **2021**, *11*, 1090. <https://doi.org/10.3390/cryst11091090>

Academic Editors: Damir Kralj, Sendhil Poornachary, Sameer Dalvi and Sébastien Teychené

Published: 7 September 2021

Publisher's Note: MDPI stays neutral with regard to jurisdictional claims in published maps and institutional affiliations.



Copyright: © 2021 by the authors. Licensee MDPI, Basel, Switzerland. This article is an open access article distributed under the terms and conditions of the Creative Commons Attribution (CC BY) license (<https://creativecommons.org/licenses/by/4.0/>).

1. Introduction

Biotechnologically produced carboxylic acids, including succinic acid (SA), are considered promising alternatives to petrochemically produced platform chemicals. The fermentative production of SA from renewable feedstocks has been demonstrated on an industrial scale, up to 30 kt a⁻¹, by different companies [1]. Traditionally, the production of succinates is conducted at neutral pH, controlled by calcium hydroxide titration. The subsequent downstream process must convert the succinates into the desired protonated form of succinic acid by adjusting the pH value by the addition of sulfuric acid, resulting in a more than equimolar side production of calcium sulfate (gypsum). This waste salt production comes along with additional costs for further treatment or disposal of the salt. Therefore, different strategies have been derived on an industrial scale to reduce, recycle or avoid waste salt production, such as low-pH fermentation processes, thermal salt cracking processes or electrochemical pH swing processes [1]. Electrified downstream concepts, which use water electrolysis to control the pH value instead of acids and bases, have shown promising results in subsequent purification of fermentation broths or in in situ processes without additional waste salt production [2–6]. Previous works have presented feasibility studies of electrochemically induced crystallization processes, which use a pH-shift to convert disodium succinate to succinic acid and to eventually crystallize the protonated succinic acid [7,8].

In order to control the electrochemically induced pH-shift crystallization process, to ensure stable operation and a certain product quality (such as, for example, a desired uniform crystal size distribution), excessive nucleation during the process should be avoided [9].

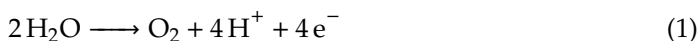
Furthermore, a well defined crystalline product can facilitate further process steps such as, for example, filtration, drying or washing. Therefore, industrial crystallization processes usually are operated within the metastable zone [9,10]. The metastable zone is defined as the region between the solid–liquid equilibrium and detection of nucleation events. It is influenced by operation parameters including saturation temperature, saturation pH, rate of supersaturation generation, composition of the solution, reactor geometry, solution history, mixing and nucleation detection method [9–12]. Hence, the measured metastable zone widths (MSZWs) are always specific for a given system and experimental setup, and can only be transferred to similar crystallization processes [13,14]. The MSZW can be used to determine nucleation kinetics for the investigated setup and system [15]. Thus, the investigation of the MSZW of electrochemically induced crystallization processes is crucial for further understanding and development of electrochemically induced crystallization.

Different measurement techniques have been used in the literature to detect nucleation, either based on a change in the physical properties of the mother solution, for example by infrared spectroscopy, ultrasound or conductivity, or based on optical detection of the grown nuclei, such as by naked eye methods, imaging procedures, turbidity or focused beam reflectance measurement [13,14,16]. However, most of these detection methods are not suitable for electrochemically induced crystallization processes due to the emerging gas phase, which disturbs the measurement signal. Therefore, an optical approach with a borescope probe was chosen for the determination of the MSZW for electrochemically induced crystallization processes in order to differentiate between the evolving gas and solid phases. The influence of current density and saturation pH on the MSZW for the electrochemically induced pH-shift crystallization was investigated. These parameters are comparable to cooling rate and saturation temperature, which are commonly investigated, for MSZWs of cooling crystallization [9,13,15]. Subsequently, an estimation of nucleation kinetics from the MSZW data was conducted by adapting the classical nucleation theory of Nývlt, developed for cooling crystallization, to electrochemically induced pH-shift crystallization [15,17].

2. Theory

2.1. Electrochemically Induced pH-Shift Crystallization

If two electrodes, an anode and a cathode, are placed in a conductive aqueous environment and a sufficient electrical potential is applied, water is split. At the anode, water is converted into oxygen and protons H^+ (Equation (1)), while at the cathode, hydrogen and hydroxide ions OH^- are produced (Equation (2)).



If the aqueous environment contains additional ions such as K^+ , Na^+ or SO_4^{2-} , which can migrate between the two electrodes, the H^+ and OH^- ions can remain in the vicinity of the respective electrode. The amount of H^+ ions n_{H^+} produced by water splitting electrolysis at the anode can be calculated by Faraday's law [18]:

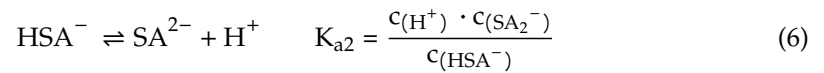
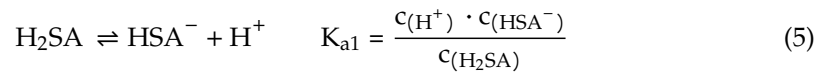
$$n_{H^+,el} = \frac{I t}{z F} \quad (3)$$

In Equation (3), I is the electric current, t is the time, z is the number of electrons transferred in the electrochemical reaction and F is the Faraday constant. The simplified definition of the pH value solely depends on the concentration of H^+ ions:

$$pH = -\log_{10}(c_{(H^+)}) \quad (4)$$

Thus, the pH (Equation (4)) is lowered at the anode and increased at the cathode by electrochemical water splitting (Equations (1) and (2)). This pH-shift influences the

dissociation of succinic acid, which can dissociate twice due to two carboxylic functional groups. Succinic acid is present either as dissociated HSA^- , SA_2^{2-} or protonated H_2SA species in the solution. Consequently, the pH value defines the amount of the different species present in the solution. The dissociation equilibrium constants $K_{a1,a2}$ for succinic acid at room temperature are reported to be $\text{p}K_{a1,a2} = -\log_{10}(K_{a1,a2}) = 4.16$ and 5.61.



The protonated species H_2SA dominates at pH values below $\text{p}K_{a1}$. Furthermore, the solubility of the protonated species differs from the dissociated species. In the case of sodium succinates the protonated species is less soluble. Hence, pH values smaller than $\text{p}K_{a1}$ are targeted for the electrochemically induced crystallization in order to generate supersaturation and produce the protonated succinic acid (Figure 1).

The driving force for the crystallization is supersaturation, which is defined by:

$$\sigma = \frac{\Delta c_i}{c_i^*} = \frac{c_i - c_i^*}{c_i^*} = S - 1. \quad (7)$$

σ is the relative supersaturation, S is the supersaturation ratio, Δc_i is the absolute supersaturation of compound i , c_i is the molar concentration of the compound i and c_i^* is the molar solubility concentration of the compound i . For succinic acid, this definition leads to 3 different supersaturations, one for each species. The supersaturated species can crystallize [19]. However, usually the solubility concentration is reported as a summation of all species concentrations over the pH, often referred to as pH-dependent solubility [20], allowing incorporation of the dissociation (Equations (5) and (6)) and the solubility of all species into one value c^* for a given pH, temperature and composition of the solution. Furthermore, the supersaturation is also reduced to one value for the summation of all succinic acid species. In this work, all concentrations are given as the summation of the succinic acid species in mol per liter. Since the targeted pH-values in this work are below 4.4, only the protonated species H_2SA can crystallize [19]. Hence, if the concentration of succinic acid (c) exceeds the solubility concentration (c^*) of the protonated species, the system will be metastable and eventually nucleation will occur.

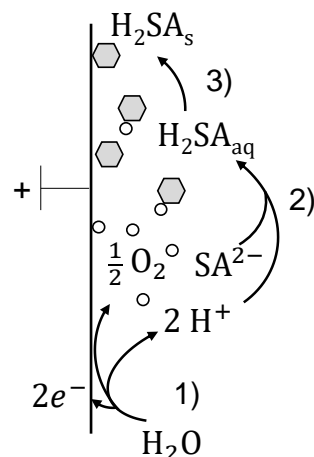


Figure 1. Nucleation in the vicinity of the anode due to an electrochemically induced acidification of the solution separated in three steps: (1) water splitting reaction, (2) protonation of the succinic acid and (3) nucleation of protonated succinic acid.

2.2. Metastable Zone Width and Determination of Nucleation Kinetics

For a system with a constantly increasing supersaturation the MZSW is used to describe the degree of a supersaturated system, which has not yet responded with nucleation [11]. The metastable zone is located between the solubility curve and the spontaneous homogeneous nucleation line. According to classical nucleation theory, the nucleation rate J_n for homogeneous nucleation can be expressed by an Arrhenius equation [10,11]:

$$J_n = A \exp\left(\frac{-B(T)}{\ln^2 S}\right). \quad (8)$$

A is a pre-exponential factor, $B(T)$ is a temperature-dependent factor and S is the supersaturation ratio (Equation (7)). However, homogeneous nucleation is often referred to as a theoretical event and heterogeneous nucleation events are far more common. Hence, the metastable zone is usually measured between the solubility curve and the heterogeneous nucleation line (Figure 2) [10–12]. Since heterogeneous nucleation events depend on the operating and experimental conditions as well as on characteristics of the investigated system, the MSZW does accordingly. The MSZW is, amongst others, affected by the rate of supersaturation generation, impurities and the surface available for heterogeneous nucleation [9]. If the surface of the solute, succinic acid, is already present, secondary nucleation events can occur. Secondary nucleation requires less supersaturation compared to primary nucleation events because it is energetically more favorable to form a stable nucleus at the surface of the solute itself. Consequently, the MZSW is narrower compared to primary nucleation (Figure 2) [9–11]. In the case of electrochemically induced crystallization the rate of supersaturation generation is controlled by the H^+ production rate of the electrolysis. An empirical relation between the nucleation rate J_n and the absolute supersaturation Δc can be derived from classical nucleation theory (Equation (8)) [9,10,15,21,22]:

$$J = k_b \Delta c^m. \quad (9)$$

The exponent m is referred to as the nucleation order and k_b is the nucleation rate constant. Both parameters have no physical meaning [10,15].

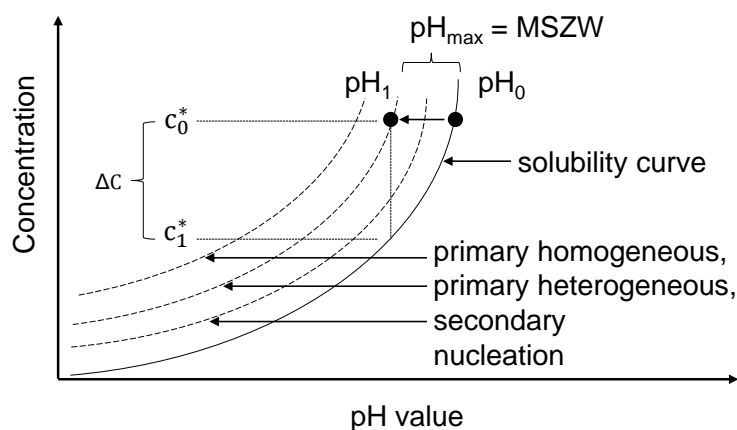


Figure 2. Metastable zone width and nucleation theory adapted to electrochemically induced pH-shift crystallization [9,12].

In analogy to the classical approach of Nývlt, the variation of supersaturation $\frac{d\Delta c}{dt}$ can be expressed, in the case of electrochemically induced pH-shift crystallization, by the rate of changing the pH value R at a given saturation pH and the corresponding slope of the pH-dependent solubility curve $\frac{dc^*}{dpH}$ [15,17]:

$$\frac{d\Delta c}{dt} = R \frac{dc^*}{dpH} = \frac{dpH}{dt} \frac{dc^*}{dpH}. \quad (10)$$

When nucleation occurs, the maximum pH difference $\Delta\text{pH}_{\text{max}}$

$$\Delta\text{pH}_{\text{max}} = \text{pH}_0 - \text{pH}_1 \quad (11)$$

and the maximum supersaturation Δc_{max} are related via the slope of the solubility curve:

$$\Delta c_{\text{max}} = \left(\frac{dc^*}{d\text{pH}} \right) \Delta\text{pH}_{\text{max}}. \quad (12)$$

Assuming that at the moment when the first nuclei is formed, the rate of generating supersaturation R is equal to the rate of nucleation J , leads to:

$$\frac{dn}{dt} = \frac{k_b \alpha \rho r^3}{M_{SA}} \Delta c^m = k(\Delta c_{\text{max}})^m. \quad (13)$$

In Equation (13), n is the molar amount of nuclei formed, M is the molar mass of succinic acid and k is the mole-based nucleation rate constant with the volume shape factor α , the crystal density ρ and the radius of the nuclei formed r . Equations (10), (12) and (13) lead to:

$$k(\Delta c_{\text{max}})^m = k \left[\left(\frac{dc^*}{d\text{pH}} \right) \Delta\text{pH}_{\text{max}} \right]^m = R \frac{dc^*}{d\text{pH}}. \quad (14)$$

This equation can be linearized to the following expression:

$$\log(R) = m \log(\Delta\text{pH}_{\text{max}}) + \log(k) + (m - 1) \log\left(\frac{dc^*}{d\text{pH}} \right). \quad (15)$$

Thus, plotting $\log(R)$ over the MSZW ($\Delta\text{pH}_{\text{max}}$), the slope of the resulting straight line is the nucleation order m and the y -intercept can be used to calculate the nucleation rate k . Using Equation (15) with the measured MSZW data allows an estimation of nucleation kinetics for the electrochemically induced crystallization.

3. Materials and Methods

3.1. Chemicals

Succinic acid ($\text{C}_4\text{H}_6\text{O}_4$) with a purity of 99% from Alfa Aesar (Kandel, Germany), di-sodium succinate ($\text{Na}_2\text{C}_4\text{H}_4\text{O}_4$) with a purity of 96% from Merck KGaA (Darmstadt, Germany), sodium sulfate (Na_2SO_4) and sodium hydroxide (NaOH) both with a purity of 99.4% supplied by VWR chemicals (Langenfeld, Germany) were used for the experimental procedures.

3.2. Analytical Procedure

In order to determine the concentration of succinic acid, samples were drawn from the solution. After filtration with a syringe filter Chromafil Xtra H-PTFE-20/13 by Macherey-Nagel (Düren, Germany), the samples were diluted with distilled water in the ratio 1:4. The concentration of succinic acid in each sample was determined by an Agilent (Ratingen, Germany) 1100 series HPLC, equipped with an organic acid resin column (250 mm \times 8 mm, LC-OrganicAcid-CS-S, CS Chromatography, Langerwehe, Germany) operated at 40 °C. A refractive index detector (RID) G1362A was used to record the SA signal. The elution was carried out with a 10 mM aqueous sulfuric acid solution and a flowrate of 0.7 mL min⁻¹. Sample injection volume was 5 μL . The pH value was measured with a FiveEasy pH meter by Mettler Toledo (Gießen, Germany).

3.3. Solubility Measurements

The solubility curves were determined at two different electrolyte concentrations, 0 M and 0.5 M Na₂SO₄. Solutions at the respective Na₂SO₄ concentrations were prepared with distilled water. After dissolution of the sodium sulfate, succinic acid and di-sodium succinate were added in different ratios to obtain different pH values. A solid phase always remained in the solution in order to ensure a saturated aqueous phase. After preparation, the solutions were mixed for 24 h and tempered in a water bath at temperature of 20 °C. The pH value of each solution and the concentration of succinic acid was measured as described above.

3.4. Determination of the Metastable Zone Width

For the determination of the MSZW, the solutions were prepared with an electrolyte concentration of 0.5 M Na₂SO₄ and pH values of 3.4, 3.6, 3.9 and 4.1, in the same manner as the solutions for the determination of the solubility curves to ensure that each experiment started with a saturated solution. After 24 h in a tempered water bath, the solid phase in the solution was separated by vacuum filtration with MN 640 w filter paper supplied by Macherey-Nagel (Düren, Germany). Furthermore, a sample was taken to measure the pH value as well as the concentration of succinic acid. The experimental setup for the determination of the metastable zone width is shown in Figure 3. The H-Cell is a double-walled glass reactor (1) with a maximal filling volume of 500 mL. It consists of an anode chamber with a ruthenium-coated titanium electrode (3) and a cathode chamber with a nickel electrode (4). The chambers are separated by a cation-exchange membrane Nafion PFSA N-117 (2) from DuPont (Wilmington, United States) between two glass fiber filters of grade 693 supplied by VWR (Langenfeld, Germany) to avoid mixing of the chambers. The power source (5) PSI 9040-20 T from Elektro-Automatik (Viersen, Germany) is connected to the electrodes, with a maximal output voltage of 40 V/DC. Two operating points, at the operational boundaries of the chosen setup, were selected for the MSZW measurement, which supplied a sufficient voltage for water splitting (>1.23 V) and stayed below 40 V. A low current density of 50 A m⁻² with a corresponding voltage of 5–7 V and a high current density of 500 A m⁻² resulting in a voltage of 37–39 V were chosen. To measure temperature and pH value, a pHenomenal 221 (VWR, Langenfeld, Germany) electrode (6) in the anode chamber is used connected to the pHenomenal 2100L pH meter by VWR (Langenfeld, Germany) with an accuracy of ±0.001 pH units. A borescope R100 038 000 50 (7) from Olympus (Shinjuku, Japan) is pointed at the anode to take pictures of the forming crystals. A clear distinction between gas bubbles and crystals is possible for a particle size of approximately 50–100 µm. Both chambers are stirred by magnetic stirrers (8) (VWR, VMS-C7 advanced); for all experiments the same stirring rate of 250 rpm was used. A thermostat (9) RC 2 basic supplied by IKA (Staufen, Germany) is used to control the temperature. For each experiment three-hundred milliliters of the solution was filled into the chambers and tempered at 20 °C. After the activation of the power source, the pH value decreased in the anode chamber and crystals occurred at the side of the anode that was facing the cathode chamber. As soon as crystals were detected by the borescope probe, pictures were taken and the current was switched off. Additionally, the solution from the anode chamber was sampled and the pH value measured in order to determine the rate of supersaturation generation R (Equation (10)).

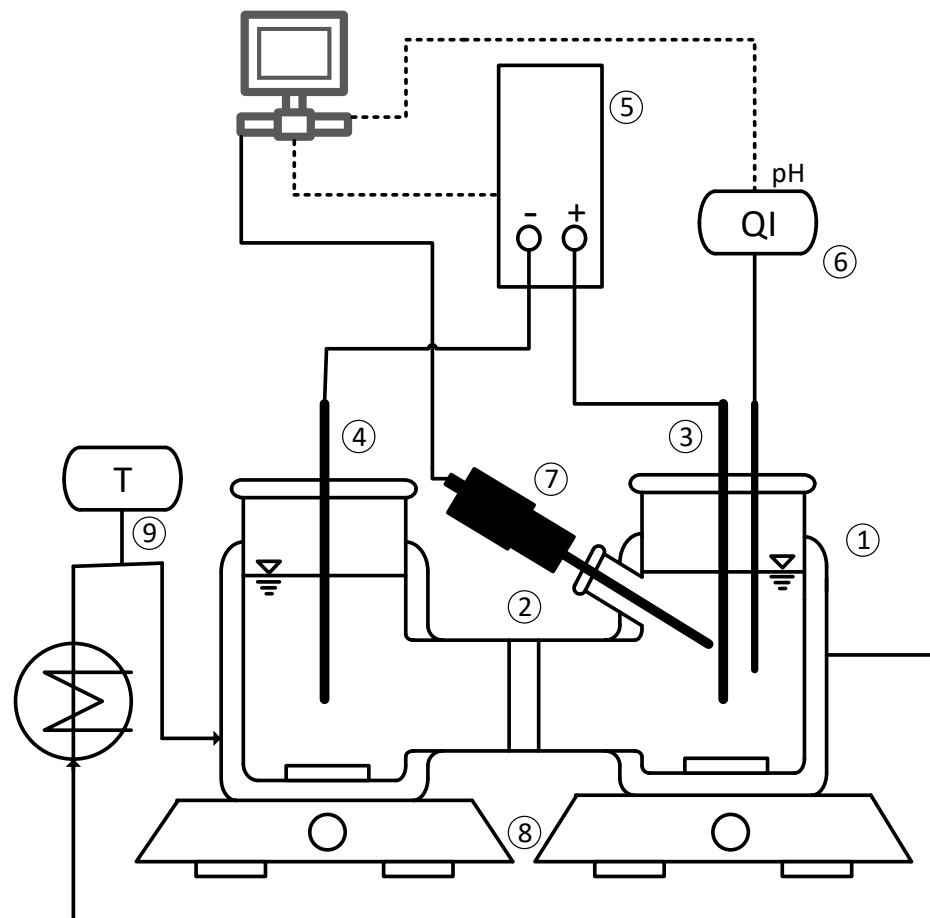


Figure 3. Experimental setup for the determination of the MSZW: (1) H-cell, (2) cation-exchange membrane, (3) anode, (4) cathode, (5) power source, (6) pH probe, (7) endoscope, (8) magnetic stirrers and (9) thermostat.

4. Results and Discussion

For the determination and the evaluation of MSZWs, the knowledge of the solubility curve is essential. It defines the solubility of succinic acid at a given temperature, pH value and composition of the solution. Furthermore, the solubility curve determines the maximum possible yield of a crystallization process [10,11]. Figure 4 shows the pH-dependent solubility curve of succinic acid in water and in an aqueous 0.5 M Na₂SO₄ solution at 20 °C.

The concentration displayed in Figure 4 is the summation of all succinic acid species. It can be seen that the solubility of succinic acid increases with increasing pH. The rising solubility can be explained by the dissociation of succinic acid, which leads to an increased amount of the dissociated species at higher pH values. The dissociated succinic acid species, in this case sodium salts of succinic acid, are more soluble than the protonated form of succinic acid, which is why the total solubility concentration of succinic acid increases towards higher pH values [19,20,25]. Furthermore, the solubility concentration decreases with increasing sodium sulfate concentration due to a higher ionic strength of the solution [20]. A similar effect is used for protein precipitation and is well known as salting out. The reduction of the solubility is a favorable side effect of the necessary electrolyte for the electrochemically induced crystallization because it reduces the solubility of the target acid, which allows a higher recovery. The measured solubility data were fitted by the MATLAB Curve Fitting toolbox to the following equation:

$$c^* = A_{\text{SOL}} \cdot \text{pH}^{\text{BSOL}} + C_{\text{SOL}}. \quad (16)$$

A_{SOL} , B_{SOL} are fit parameters. The parameter C_{SOL} is the intrinsic solubility concentration of the protonated succinic acid, since at low pH values (around 0) $C_{SOL} = c_{H_2SA}^*$ represents the solubility concentration (Table 1).

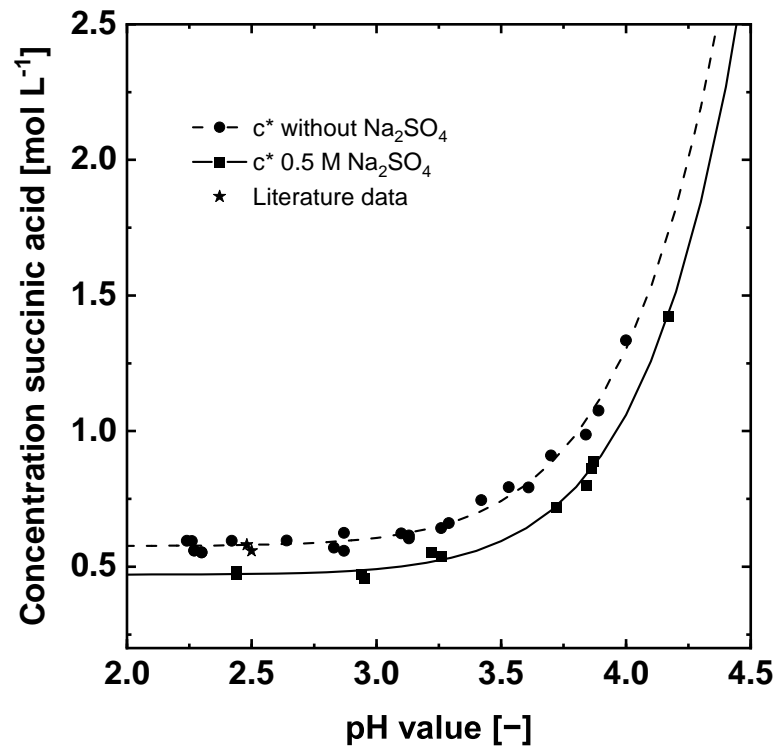


Figure 4. Influence of the pH value and sodium sulfate on the solubility of succinic acid at 20 °C. Symbols (■ ●) are measured concentrations and lines are calculated by Equation (16). The literature data (★) are calculated from [23,24].

Table 1. Solubility curve parameters fitted to Equation (16) for succinic acid.

Na_2SO_4	A_{SOL}	B_{SOL}	C_{SOL}	R^2
0 M	1.571×10^{-7}	11.07	0.576	0.983
0.5 M	5.249×10^{-8}	11.71	0.471	0.997

The measured solubility concentrations are in good agreement with the literature data in water at 20 °C [23,24] (Figure 4).

The measured MSZWs for two different current densities are presented together with the respective solubility curves in Figure 5. The MSZWs are narrow for both current densities. For 50 A m⁻² the MSZW ranges between 0.01 and 0.05 pH units. For a tenfold higher current of 500 A m⁻² the MSZW lies between 0.02 and 0.08 pH units. The nucleation occurred exclusively in the vicinity of the anode and on the electrode surface (Figure 5). Two factors accelerate the nucleation in the vicinity of the anode. First, in this region of the H-Cell reactor foreign surfaces are present in the form of the anode and oxygen bubbles produced by the water splitting reaction. Foreign surfaces can act as nucleation sites by reducing the necessary nucleation energy needed to form a stable crystal cluster [11,16,26]. Second, the supersaturation close to the anode surface is higher compared to the solution further away, due to the production of H⁺ ions and consequently lower pH value. This leads to a higher possibility of nucleation in this region compared to regions further away from the anode [27].

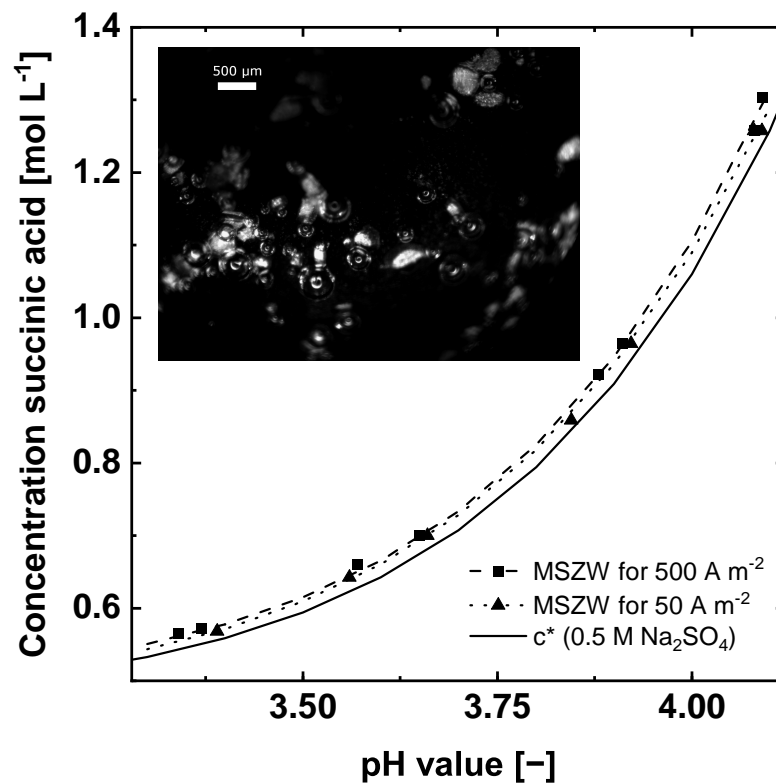


Figure 5. MSZWs of succinic acid for different current densities (■ ▲) along the solubility curve (Equation (16)). An exemplary image of the detected nucleation on the surface of the anode obtained with the borescope probe.

Figure 6 displays the MSZW, $\Delta\text{pH}_{\text{max}}$ and the corresponding relative supersaturation. As expected, an increase in the current density leads to a wider MSZW (Figure 6). Similar to, e.g., cooling crystallization, increasing the supersaturation generation rate leads to wider MSZW because the system has less time at a given supersaturation to develop stable nuclei [9,11,28]. The increasing MSZW due to higher supersaturation generation rates is commonly explained by the existence of the induction period, which is the time span between the occurrence of the supersaturation and the formation and growth of nuclei to detectable size [10]. For fast supersaturation generation rates, the phase transformation lags behind the supersaturation generation rate leading to a higher supersaturation, and consequently larger MSZW, at the time the nuclei are detected. Hence, at low supersaturation generation rates the nuclei are detected at lower maximal supersaturation [29,30]. Furthermore, a higher current leads consequently to more gas phase (Equation (1)), which could serve as a nucleation site. However, this was not observed in the experiments. More gas phase, due to a higher current density, does not lead to a further reduction of the MSZW (Figure 6). For the investigated range of current densities the amount of introduced gas bubbles had no significant influence on the MSZW. The induced volume flow of oxygen at the anode can be calculated by Equation (3) to $2.32 \times 10^{-5} \text{ L s}^{-1}$ and $2.32 \times 10^{-4} \text{ L s}^{-1}$, which is small compared to the filling volume of 0.3 L. The hold-up in the vicinity of anode cannot be measured or calculated with the methods described above. However, it seems essential for the observed nucleation process that a foreign surface in form of gas bubbles is present in the area of the reactor where the supersaturation is the highest (close to the anode). This matches well with the literature on gassed cooling crystallization [23,26], which stated that the way of introducing gas bubbles and the amount and duration of gassing during a cooling crystallization had no significant influence on the nucleation (induction time). However, there was a significant reduction in the induction time, and an accelerated nucleation, compared to experiments without gassing [23,26]. Furthermore, the MSZW decreases with increasing saturation concentration and pH value. Higher

saturation concentrations increase the statistical chance of forming stable nuclei, due to a higher concentration of monomers, resulting in an earlier nucleation and consequently in a narrower MSZW [10,11]. Hence, the faster nucleation at higher saturation concentrations is a kinetic effect due to a higher amount of available building blocks for stable nuclei and not due to higher supersaturation. Figure 6 underlines this assumption; the relative supersaturation did not change significantly for different saturation concentrations at a given current density. However, for different driving forces of the electrochemically induced crystallization, the applied current density, the supersaturation varied. For 50 A m^{-2} , the average supersaturation was approx. $\sigma = 0.027$, and for 500 A m^{-2} , an average relative supersaturation of approx. $\sigma = 0.045$ was reached (Figure 6).

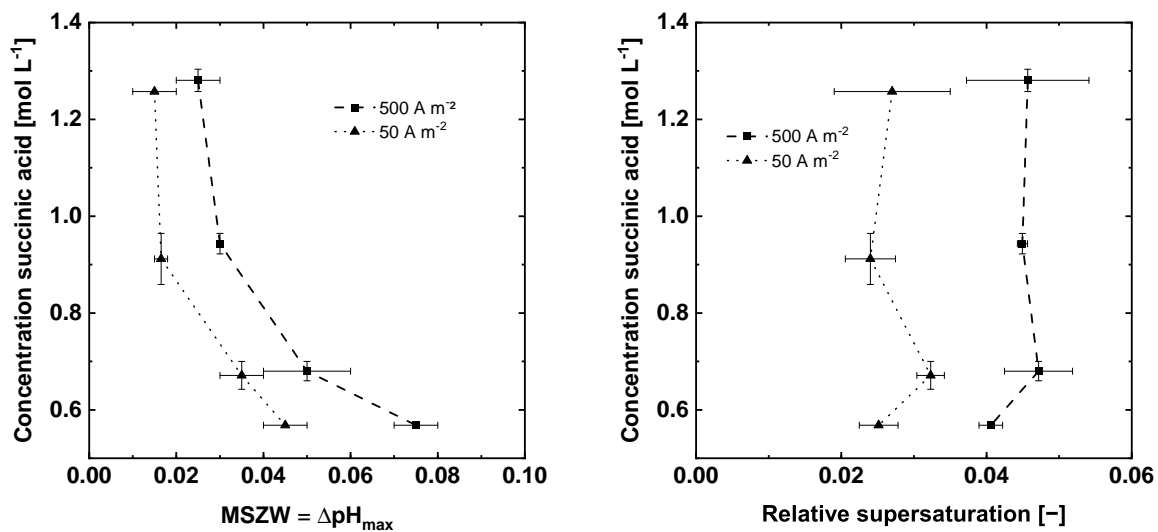


Figure 6. Effect of the applied current density and saturation concentration on the MSZW of succinic acid and on the reachable supersaturation. Dots are measured concentrations, pH values respective calculated supersaturations (■ ▲).

Equation (15) allows an estimation of the nucleation kinetic by plotting the rate of changing the pH value R versus the MSZW (Figure 7). The nucleation order m is the slope of the straight fits shown in Figure 7 and the nucleation rate constant k is calculated from the y-intercept and the slope of the solubility curve at the saturation pH value $\frac{dc^*}{dpH}$ listed in Table 2.

Table 2. Determined nucleation parameters of succinic acid for electrochemically induced pH-shift crystallization.

Saturation pH Value	m	y-Intercept	$\frac{dc^*}{dpH}$	k
4.1	4.984	3.610	2.247	161.953
3.9	4.861	2.867	1.315	267.308
3.6	4.731	1.806	0.558	563.780
3.4	3.901	0.409	0.303	44.659

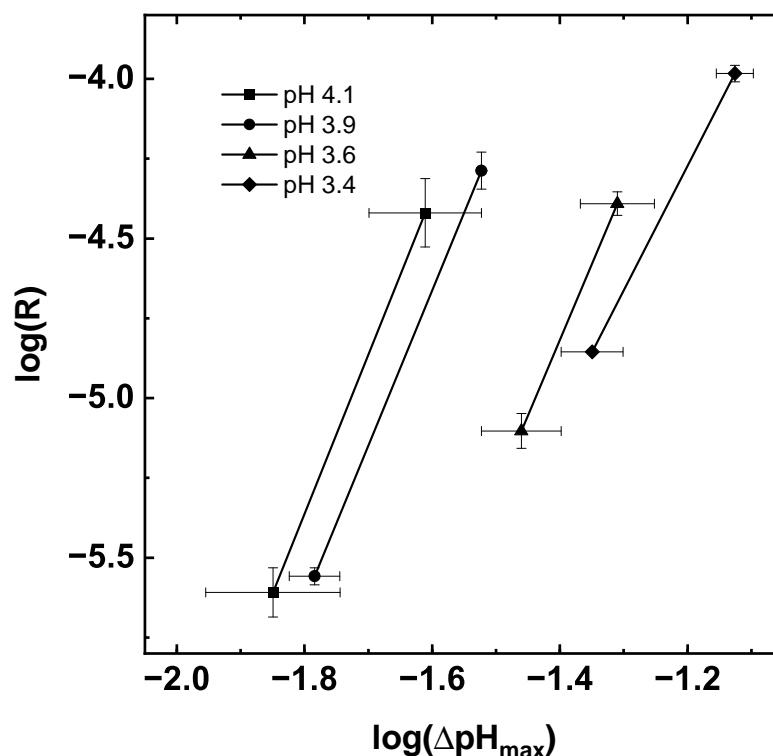


Figure 7. Logarithmic plot of the MSZW and the measured pH shift over the experiment duration $R_{\text{total}} = \frac{\Delta\text{pH}}{\Delta t}$ for experiments with different saturation pH values. The points were calculated by the averaged MSZW and R_{total} of two experiments. Straight line fits were used to estimate the kinetic nucleation parameters.

The nucleation order m remains in a similar order of magnitude while the nucleation rate constant varies for the different saturation pH values, which could indicate a change in the nucleation mechanism at low saturation pH values [16]. Furthermore, the nucleation order m for succinic acid is comparable with the literature data for gassed cooling nucleation [16]. This underlines that the nucleation mechanisms measured for the electrochemically induced crystallization are similar to gassed cooling crystallization, which is likely induced by a foreign surface. However, due to a different crystallization process, pH-shift instead of cooling, composition of the solution (Na_2SO_4) and detection technique of the MSZW, the nucleation rate constant k cannot be compared [14,15]. Furthermore, the kinetic parameters in Table 2 were calculated from data for two operating points for each pH value due to the limits of the experimental setup (compare Section 3.4). For further investigation of nucleation processes for electrochemically induced crystallization of succinic acid, an even wider range of operating parameters and different electrochemical cell types, with smaller electrode gaps such as stack modules, should be envisaged.

5. Conclusions

Within this work an experimental method to evaluate the MSZW for electrochemically induced pH-shift crystallization processes was developed. A borescope probe was used to determine the MSZW of succinic acid in aqueous Na_2SO_4 solutions. The effects of the initial saturation concentration as well as the applied electrical current density on the MSZW were studied. The consistently observed narrow MSZWs indicate that nucleation due to foreign surfaces, the electrode and gas phase evolving at the electrode, within electrochemically induced crystallization processes is practically inevitable. This might pose challenges in achieving well-defined product size distribution at a large scale, since in a large scale higher current densities are envisaged and additional fluctuations are expected in the case of continuously operated crystallization processes. However, a continuous generation of

crystals by nucleation can be beneficial for stable operating conditions in continuously operated crystallization processes [11].

The obtained MSZWs were used to estimate kinetic nucleation parameters adapting the classical nucleation theory to the electrochemically induced crystallization concept. The obtained kinetic parameters for succinic acid underline the assumption of nucleation processes induced by foreign surfaces.

Author Contributions: C.K.: conceptualization, methodology, software, data curation, investigation, writing—original draft preparation, project administration. C.M.K.: methodology, data curation, investigation, writing—review and editing. M.G.: methodology, resources, writing—review and editing. A.J.: supervision, funding acquisition. All authors have read and agreed to the published version of the manuscript.

Funding: The authors gratefully acknowledge the financial support of “E-HyBio” as part of the BMBF project “BioökonomieREVIER” no. 031B0918A and the project supervision by the project management organization Projektträger Julich (PtJ). The support and contribution of the Kopernikus project SynErgie (03SFK3L1-2) by the Federal Ministry of Education and Research (BMBF) is recognized.

Conflicts of Interest: The authors declare no conflict of interest.

References

1. Jansen, M.L.A.; van Gulik, W.M. Towards large scale fermentative production of succinic acid. *Curr. Opin. Biotechnol.* **2014**, *30*, 190–197. [[CrossRef](#)]
2. Andersen, S.J.; Candry, P.; Basadre, T.; Khor, W.C.; Roume, H.; Hernandez-Sanabria, E.; Coma, M.; Rabaey, K. Electrolytic extraction drives volatile fatty acid chain elongation through lactic acid and replaces chemical pH control in thin stillage fermentation. *Biotechnol. Biofuels* **2015**, *8*, 221. [[CrossRef](#)] [[PubMed](#)]
3. Kim, Y.H.; Moon, S.H. Lactic acid recovery from fermentation broth using one-stage electrodialysis. *J. Chem. Technol. Biotechnol.* **2001**, *76*, 169–178. [[CrossRef](#)]
4. Hábová, V.; Melzoch, K.; Rychtera, M.; Sekavová, B. Electrodialysis as a useful technique for lactic acid separation from a model solution and a fermentation broth. *Desalination* **2004**, *162*, 361–372. [[CrossRef](#)]
5. Urbanus, J.; Bisselink, R.; Nijkamp, K.; ter Horst, J.H.; Verdoes, D.; Roelands, C. Integrated product removal of slightly water-soluble carboxylates from fermentation by electrochemically induced crystallization. *J. Membr. Sci.* **2010**, *363*, 36–47. [[CrossRef](#)]
6. Gausmann, M.; Kocks, C.; Pastoors, J.; Büchs, J.; Wierckx, N.; Jupke, A. Electrochemical pH-T-Swing Separation of Itaconic Acid for Zero Salt Waste Downstream Processing. *ACS Sustain. Chem. Eng.* **2021**, *9*, 9336–9347. [[CrossRef](#)]
7. Kocks, C.; Görtz, J.; Holtz, A.; Gausmann, M.; Jupke, A. Electrochemical Crystallization Concept for Succinic Acid Reduces Waste Salt Production. *Chem. Ing. Tech.* **2019**, *754*, 46. [[CrossRef](#)]
8. Gausmann, M.; Kocks, C.; Doeker, M.; Eggert, A.; Maßmann, T.; Jupke, A. Recovery of succinic acid by integrated multi-phase electrochemical pH-shift extraction and crystallization. *Sep. Purif. Technol.* **2020**, *240*, 116489. [[CrossRef](#)]
9. Ulrich, J.; Strege, C. Some aspects of the importance of metastable zone width and nucleation in industrial crystallizers. *J. Cryst. Growth* **2002**, *237–239*, 2130–2135. [[CrossRef](#)]
10. Mullin, J.W. *Crystallization*, 4th ed.; Elsevier Professional: Amsterdam, The Netherlands, 2001.
11. Beckmann, W.; Lorenz, H.; Hilficker, R.; Schmidt, C.; Jones, J., M.; Ulrich, J.; Wieckhusen, D.; Hofmann, G.; Melches, C.; Nienhaus, B.; et al. *Crystallization: Basic Concepts and Industrial Applications*; Wiley-VCH: Weinheim, Germany, 2013.
12. Mersmann, A.; Kind, M.; Stichlmair, J. *Thermische Verfahrenstechnik: Grundlagen und Methoden*, 2nd ed.; Wesentlich Erw. und Aktualisierte Aufl.; Chemische Technik Verfahrenstechnik; Springer: Berlin, Germany, 2005.
13. Barrett, P.; Glennon, B. Characterizing the Metastable Zone Width and Solubility Curve Using Lasentec FBRM and PVM. *Chem. Eng. Res. Des.* **2002**, *80*, 799–805. [[CrossRef](#)]
14. Kubota, N. A new interpretation of metastable zone widths measured for unseeded solutions. *J. Cryst. Growth* **2008**, *310*, 629–634. [[CrossRef](#)]
15. Nývlt, J. Kinetics of nucleation in solutions. *J. Cryst. Growth* **1968**, *3–4*, 377–383. [[CrossRef](#)]
16. Kleetz, T.; Pätzold, G.; Schembecker, G.; Wohlgemuth, K. Gassing Crystallization at Different Scales: Potential to Control Nucleation and Product Properties. *Cryst. Growth Des.* **2017**, *17*, 1028–1035. [[CrossRef](#)]
17. Chaitanya, K.K.; Sarkar, D. Determination of the Metastable Zone Width by a Simple Optical Probe. *Chem. Eng. Technol.* **2014**, *37*, 1037–1042. [[CrossRef](#)]
18. Schmidt, V.M. *Elektrochemische Verfahrenstechnik: Grundlagen, Reaktionstechnik, Prozessoptimierung: Grundlagen, Reaktionstechnik, Prozessoptimierung*; Wiley-VCH: Weinheim, Germany, 2003.
19. Lange, L.; Lehmkemper, K.; Sadowski, G. Predicting the Aqueous Solubility of Pharmaceutical Cocrystals As a Function of pH and Temperature. *Cryst. Growth Des.* **2016**, *16*, 2726–2740. [[CrossRef](#)]

20. Holtz, A.; Görtz, J.; Kocks, C.; Junker, M.; Jupke, A. Automated measurement of pH-dependent solid-liquid equilibria of itaconic acid and protocatechuic acid. *Fluid Phase Equilibria* **2021**, *532*, 112893. [[CrossRef](#)]
21. Sangwal, K. A novel self-consistent Nývlt-like equation for metastable zone width determined by the polythermal method. *Cryst. Res. Technol.* **2009**, *44*, 231–247. [[CrossRef](#)]
22. Nagy, Z.K.; Fujiwara, M.; Woo, X.Y.; Braatz, R.D. Determination of the Kinetic Parameters for the Crystallization of Paracetamol from Water Using Metastable Zone Width Experiments. *Ind. Eng. Chem. Res.* **2008**, *47*, 1245–1252. [[CrossRef](#)]
23. Kleetz, T.; Funke, F.; Sunderhaus, A.; Schembecker, G.; Wohlgemuth, K. Influence of Gassing Crystallization Parameters on Induction Time and Crystal Size Distribution. *Cryst. Growth Des.* **2016**, *16*, 6797–6803. [[CrossRef](#)]
24. Apelblat, A.; Manzurola, E. Solubility of oxalic, malonic, succinic, adipic, maleic, malic, citric, and tartaric acids in water from 278.15 to 338.15 K. *J. Chem. Thermodyn.* **1987**, *19*, 317–320. [[CrossRef](#)]
25. Li, Q.; Wang, D.; Wu, Y.; Li, W.; Zhang, Y.; Xing, J.; Su, Z. One step recovery of succinic acid from fermentation broths by crystallization. *Sep. Purif. Technol.* **2010**, *72*, 294–300. [[CrossRef](#)]
26. Wohlgemuth, K.; Kordylla, A.; Ruether, F.; Schembecker, G. Experimental study of the effect of bubbles on nucleation during batch cooling crystallization. *Chem. Eng. Sci.* **2009**, *64*, 4155–4163. [[CrossRef](#)]
27. Nývlt, J.; Rychlý, R.; Gottfried, J.; Wurzelová, J. Metastable zone-width of some aqueous solutions. *J. Cryst. Growth* **1970**, *6*, 151–162. [[CrossRef](#)]
28. Sangwal, K. Some features of metastable zone width of various systems determined by polythermal method. *CrystEngComm* **2011**, *13*, 489–501. [[CrossRef](#)]
29. Bian, C.; Chen, H.; Song, X.; Yu, J. Metastable zone width and the primary nucleation kinetics for cooling crystallization of NaNO₃ from NaCl-NaNO₃-H₂O system. *J. Cryst. Growth* **2019**, *518*, 5–13. [[CrossRef](#)]
30. Kulkarni, S.A.; Kadam, S.S.; Meekes, H.; Stankiewicz, A.I.; ter Horst, J.H. Crystal Nucleation Kinetics from Induction Times and Metastable Zone Widths. *Cryst. Growth Des.* **2013**, *13*, 2435–2440. [[CrossRef](#)]